Advanced Chemical Process Analysis
https://www.sciltp.com/journals/acpa

Article

Capability of Digital Twins for Representing a Complex Process—Prediction of Multicomponent Adsorption Breakthrough Curves and Times

Jose Luis Valverde [1,*], Victor Roberto Ferro [2,†], María Mercedes Romero-Díaz [1,†] and Anne Giroir-Fendler [3,†]

1 Department of Chemical Engineering, University of Castilla La Mancha, Avenida Camilo José Cela 10, 13071 Ciudad Real, Spain
2 Department of Chemical Engineering, Universidad Autónoma de Madrid, C. Francisco Tomás y Valiente 7, Fuencarral-El Pardo, 28049 Madrid, Spain
3 Department of Chemistry and Biochemistry, Université Claude Bernard Lyon 1, CNRS, IRCELYON, 2 Avenue Albert Einstein, F-69622 Villeurbanne, France
* Correspondence: joseluis.valverde@uclm.es; Tel.: +34-926-295-300
† These authors contributed equally to this work.

How To Cite: Valverde, J.L.; Ferro, V.R.; Romero-Díaz, M.M.; et al. Capability of Digital Twins for Representing a Complex Process—Prediction of Multicomponent Adsorption Breakthrough Curves and Times. *Advanced Chemical Process Analysis* **2025**, *1*(1), 2.

Received: 29 January 2025
Revised: 3 March 2025
Accepted: 4 March 2025
Published: 6 March 2025

Abstract: This work tries to elucidate the reliability of artificial neural networks (ANN) to predict complex processes. This way, breakthrough curves and breakthrough times corresponding to 243 different scenarios of the multicomponent adsorption of H_2, CO and CO_2 in a fixed bed from a large set of runs (rather than a single run, which is the majority situation reported in the literature) generated through Aspen Adsorption™, were fitted to 600 ANNs configurations through a homemade software running in Fortran and 8 additional algorithms contained in the Scikit-Learn, a Python module for machine learning. To generate a consistent ANN, data obtained through Aspen Adsorption™ were randomly divided into two groups: training (80% of the breakthrough curves and breakthrough times) and validation (20% of them). This procedure was able to properly predict single breakthrough curves. However, the capacity of the ANN for predicting a set of breakthrough curves was not so good as expected although the trends followed by the prediction curves could be used to make a good estimation of the dynamic behaviour of adsorption process. Finally, it was observed a good agreement between the values of the breakthrough times corresponding to the reduction of the H_2 concentration in the outlet stream of 2% computed by Aspen Adsorption™ and used for validation and those predicted by the best ANN model. The general procedure here followed could be equally used for analyzing real set of adsorption experiments or other different complex processes as described here.

Keywords: digital twin; multicomponent adsorption; Aspen Adsorption™

1. Introduction

Computational tools based on artificial neural networks (ANNs), which are nonlinear regression algorithms in the Machine Learning field for classification and prediction [1], have been successfully used by both academia and industry, and their use is common in Artificial Intelligence (AI). From them, it is possible to obtain a digital twin (DT), which is a virtual model created to represent processes, which can in turn be updated and maintained in real time. AI has introduced new possibilities for modeling and simulating chemical processes [2]. Industry 4.0 requires this piece of knowledge from chemical and process engineers since process plants have large volumes of stored historical data obtained through sensors that measure thousands of variables in the order of seconds [3]. Chemical engineers use ANNs in process prediction and classification when there is a lack of both physical understanding of the problem and statistical variations of the observable data [3].

Modeling, simulation, and optimization are essential activities among researchers to meet the challenges produced by environmental and commercial restrictions. In a recent paper [4], DTs based on ANNs were generated for predicting the steady state of styrene production from benzene. The data used were produced from Aspen HYSYS, which led to determining the operating conditions of pre-heating, reaction, and stabilization units. In another recent paper [5], a DT was used to obtain a virtual representation of the experimental data from an alkaline leaching process of black masses from spent batteries. For this purpose, 90% of the experimental data were used for training a supervised learning procedure involving 600 different artificial neural networks (ANNs) derived from twelve different activation functions.

A neural network contains hyperparameters to be tuned prior to training in order to achieve the best configuration. Particularly, activation functions determine the output of the model, its accuracy, and the computational efficiency of training a model; therefore, they are an essential part of the structure of neural networks. The Sigmoid function, Hyperbolic Tangent (TanH), and ReLU (Rectified Linear Unit) are the most common in Chemical Engineering, although many more have been defined [1]. A remarkable challenge is to find the best configuration of layers and activation functions that fit the data of a process.

Another important issue is to know the capability of the ANNs to predict the behaviour of a process when many independent and dependent variables are involved. In this context, the dynamics of adsorption in a fixed bed has been used for dilucidating the capability of the ANNS to describe a complex process. As observed in the literature, most of the studies are focused on the prediction of both the capacity of adsorption and the breakthrough times. Some of them are focused on the prediction of the adsorption dynamic (breakthrough curves) but consider single experiments rather than a set of experiments as proposed here.

The breakthrough time is an important factor in Pressure Swing Adsorption (PSA) cycle design and depends on the adsorption capacity at given conditions, such as temperature, composition, pressure and so on. Specifically, the breakthrough time of hydrogen is a key factor in determining the performance of PSA [6], which is a common method to obtain high-purity hydrogen. The breakthrough time can well reflect the adsorption dynamics and help PSA cycle design. In order to avoid time-consuming and labor-intensive breakthrough curve experiments, it is necessary to develop a fast and accurate surrogate model [6]. ANNs are a good candidate as demonstrated more than 20 years ago [7]. Thus, some studies have been reported for obtaining ANN-based surrogate models that are able to efficiently compute the transient adsorption behavior and breakthrough times without altering the capability of first-principles models [8].

Despite these efforts, challenges remain in studying multicomponent breakthrough curves for hydrogen purification. ANNs and interior point algorithms have been used to optimize the breakthrough time of individual gases in a three-component gas $H_2/CO/CH_4$ system [9]. This method can only ensure that the breakthrough time of CO or CH_4 is maximum but cannot guarantee that the breakthrough time of both CO and CH_4 can be maximized simultaneously.

ANNs were also applied to model the sorption of dyes blue No. 1 and red No. 2 in aqueous solutions using magnesium and aluminum double layer hydroxides (LDH) interspersed with nitrate ions [10]. Single experimental breakthrough curves were compared with data obtained in the ANN modeling, using four inputs and one output variable for each dye showing an excellent correlation (r^2 = 0. 99). Three machine learning models (random forest, support vector machine, and artificial neural network) were developed to predict the adsorption capacity of microplastics [11]. The ANN model has been widely used to predict pollutant adsorption in fixed beds under different operating parameters in the treatment of pollutants [12–15]. Modified biochar was used in the adsorption performance of sulfamethoxazole [16]. Based on batch experiment results, an artificial neural network (ANN) model was developed to describe the adsorption data of this pollutant sufficiently (r^2 > 0.99). Also, ANNs have been used to describe the adsorption of Cr(VI) from aqueous solutions using activated carbon produced from waste tires [17]. The conjugate gradient backpropagation algorithm was found to be the best training one among all the training algorithms, with a root mean squared error (RSME) of 5.894 and an r^2 of 0.985. The dynamic of the tetracycline adsorption process using raw rice husk was also modeled using ANNs with a correlation coefficient of 0.999 [18].

In a review reported recently, the use of ANNs for evaluating isothermal, kinetic, and thermodynamic parameters in multicomponent adsorption on biomaterials was discussed [19]. The cyclohexane and n-hexane adsorption capacity over graphene was analyzed with a neural network, which was able to predict the experimental values with a correlation coefficient of 0.99966 [20]. In other reviews, the modeling of adsorption of organic and inorganic pollutants from water using ANNs [19,21,22] was reported. ANNs were also used to emulate adsorption and chromatography processes [23]. The proposed approach focuses on learning the underlying governing partial differential equations in the form of a physics-constrained loss function to simulate adsorption processes accurately. The results demonstrated that the purity and recovery calculated from the neural network-based simulations were within 2.5% of the detailed model predictions. A deep learning artificial neural network framework was also used to optimize the adsorption capacity of 3-nitrophenol using carbonaceous material obtained from biomass wastes [24]. An artificial neural network (ANN) model was improved to estimate the efficiency of Cr(III) and Cr(VI) ions adsorption in aqueous solution on natural, acid-activated and base-activated cherry stalks [25]. A modeling study using ANNs was performed in adsorptive removal of Congo Red on activated hazelnut [26], revealing a correlation of 98%. An ANN model was also able to predict with a higher coefficient of determination and lower root mean square error values the adsorption capacity of organic waste-derived carbon-based materials as a function of the. adsorbent synthesis conditions, adsorbent physical characteristics and adsorption experimental conditions [27]. Feature importance using Shapley additive explanations analysis suggested that the adsorption characteristics with 51.4% were the most important in the ANN prediction. Many more studies have been reported that use ANNs for the prediction of adsorption processes: CO_2 adsorption in metal-organic frameworks (MOFs) [28], silicic acid removal in a fixed-bed column using a modified resin [29], fluoride removal efficiency using neutralized activated red mud from aqueous medium in a continuous fixed bed column [30], time allocation of a three-bed adsorption chiller using an ANN [31], competitive adsorption of dyes on Gemini Polymeric nanoarchitecture [32], fixed-bed phenolic compounds adsorption onto activated date palm biochar [33], mercury adsorption by a dendrimer-grafted polyacrylonitrile fiber in fixed-bed column [34], organic pollutants adsorption on activated carbon [35], adsorption of sunset yellow onto neodymium modified ordered mesoporous carbon [36], Cu(II) adsorption from an aqueous solution [37], heavy metals adsorption dynamic on surfactant decorated graphene [14], color adsorption from an industrial textile effluent using modified sugarcane bagasse [38], asphaltenes adsorption by nanocomposites [39], adsorption of methylene blue in a fixed bed column [40], Pb(II) adsorption [41,42], malachite green adsorption by tea waste [43], Cr(VI) adsorption from aqueous solution with Aliquat 336-derived adsorbents [44], Ni(II) adsorption from aqueous solution by peanut shell [45], Sr(II) adsorption from aqueous solution by natural calcium-based materials [46], and adsorption chromatography of chitosanases produced by Paenibacillus ehimensis [47], among others.

On the other hand, Aspen Adsorption^{TM}, which is integrated into the AspenTech software, is a very powerful tool for simulating adsorption processes. Aspen Adsorption enables process simulation and optimization for a wide range of industrial gas and liquid adsorption processes, including reactive adsorption, ion exchange, and cyclic processes. Despite that few studies are using Aspen Adsorption^{TM} as a tool for simulating adsorption processes [48]. Some examples have been reported in the literature: a single bed Pressure Swing Adsorption (PSA) unit for the carbon capture process of CO_2 and H_2 [48], different configuration of adsorption units including pressure swing ones [49], six-step pressure swing adsorption process for biogas separation on a commercial scale [50], etc. In a recent study [51], an ANN was used to optimize a six-step two-bed pressure swing adsorption system for hydrogen purification. The pressure swing adsorption model used for describing the hydrogen purification was developed on the Aspen/Adsorption software platform.

This work tries to elucidate the reliability of ANNs to predict a complex process. Thus, the dynamics of a set of experiments of adsorption in a fixed bed were considered. As mentioned above, this study faces the capability of the ANNs to predict both the breakthrough curves and the breakthrough times of multicomponent adsorption in a fixed bed from a large set of runs (rather than a single run, which is the majority situation reported in the literature) generated through Aspen Adsorption^{TM}. The system considered was constituted by a stream containing H_2, CO and CO_2. Basic data for performing the simulation was taken and adapted from the literature [52]. The adsorbent used was a mixture with the same amount by weight of zeolite and activated carbon. From that, 243 different scenarios were generated with the software mentioned above. From them, it was selected sets of data depending of the ending time of the simulation: 25, 50, 100 and 200 s. The different sets were fitted to 600 ANNs configurations through homemade software running in Fortran. Eight additional algorithms contained in the Scikit-Learn, a Python module for machine learning: Linear regression, Ridge, Lasso, Lars, LassoLars, MultiTaskElasticNet, and OrthogonalMatchingPursuit, were also considered. An MS Escel-VBA application was built to control the data transfer from this application to the Fortran and Python ones. Data collected were compared and the best results were selected. Regarding the input variables, seven were considered in this study: time on stream, compositions in molar fraction of methane, carbon monoxide and hydrogen, and pressure at the inlet stream to the process and the height and diameter of the bed. Three output variables were considered: molar fractions of methane, carbon monoxide and hydrogen at the effluent stream of the process. To generate a consistent ANN, the data obtained through Aspen Adsorption^{TM} was randomly divided into two groups: (i) 80% of the breakthrough curves and breakthrough times, which were used for ANNs training, and (ii) 20% of them, which were used for validation.

2. Materials and Methods

2.1. Aspen Adsorption™

Aspen Adsorption™ was used for generating the 243 scenarios mentioned above. Before running a scenario, a set of steps should be followed (Figures S1–S5): fluid package definition (Peng-Robinson) and components selection (CH_4, CO and H_2), simulation mode definition (in this case "Gas Dynamic"), blocks selection (the main one is "Gas Bed"), and configuration of the geometric properties of the bed and its layers. Figure 1 shows the final flowsheet used in the simulation.

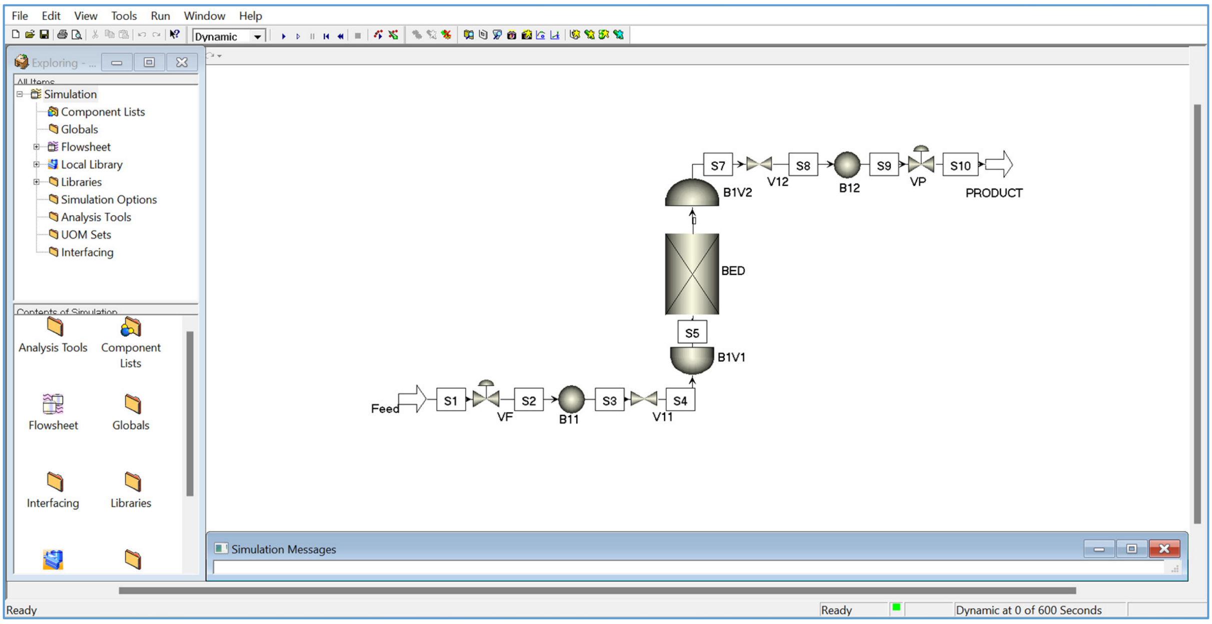

Figure 1. Flowsheet used for the simulation of a fixed bed with Aspen Adsorption™. Data of the seven input variables and the three output variables were recorded each second of the simulation run.

2.2. ANNs

In a previous work [5], the procedure for training and validating models here followed is described, which is more extensively explained in the Supplementary Materials section. Apart from the seven activation functions listed in Table 1 [4,53–57], additional models taken from the Python module for machine learning Scikit-Learn (https://scikit-learn.org/stable/, accessed on 15 January 2025): Linear regression, Ridge, Lasso, Lars, LassoLars, MultiTaskElasticNet, and OrthogonalMatchingPursuit, were also considered. In the input layer, the number of input variables (independent variables) fixed the number of neurons of the layer, whereas in the output layer, the numbers of neurons were fixed by the number of output variables (dependent variables). One or two hidden layers were considered. In this way, the neural network learning capacity was determined by the number of hidden layers as well as the neurons contained in each layer. By combining the seven activation functions listed in Table 1 and considering 2 or 3 layers, 600 different configurations could be defined. An MS Excel-VBA application (register number TXu 2-443-000 of the Copyright Office of USA) was built to control the data transfer from this application to other two (system model): an executable file generated from a Fortran code which sped up the numerical computations of the 600 models derived from Table 1, and an script written in Python to run the 8 models included in the Scikit-Learn module. The MS Excel-VBA collected the results generated by these two applications and performed the fitting and validation processes of all the models considered here. Adding up the functions considered from Scikit-Learn, the total number of models tested was 608. Seven input variables were considered in this study: time on stream, compositions in molar fraction of methane, carbon monoxide and hydrogen, and pressure at the inlet stream to the process and the height and diameter of the bed. Three output variables were considered: molar fractions of methane, carbon monoxide and hydrogen at the effluent stream of the process.

Table 1. Activation functions used in this study for generating ANNs [4,53–57].

Activation Function	ID Code	Mathematical Expression
Log-Sigmoid	LOGSIG	$a_j = \frac{1}{1+e^{-n_j}}$
Hyperbolic Tangent Sigmoid	HTANSIG	$a_j = \frac{e^{n_j} - e^{-n_j}}{e^{n_j} + e^{-n_j}}$
Linear	LINEAR	$a_j = n_j$
Swish	SWISH	$a_j = \frac{n_j}{1+e^{-n_j}}$
ELU	ELU	$a_j = \begin{cases} \alpha(e^{n_j} - 1) & n_j < 0 \\ n_j & n_j \geq 0 \end{cases}$
RELU	RELU	$a_j = \begin{cases} 0.01 n_j & n_j \leq 0 \\ n_j & n_j > 0 \end{cases}$
Polynomial *	POL	$a_j = n_j^i$

* where *i* is in the range from 1 to the total neurons in layer *j*.

The training process was performed by minimizing the function χ_j^2 by nonlinear regression by using the Levenberg-Marquardt algorithm [58]:

$$\chi_j^2 = \sum_{i=1}^{m} \left[\sum_{k=1}^{n} \left(y_{ik} - a_{ikj}^s \right)^2 \right] \quad (1)$$

where m is the number of experiments, n is the number of output variables, y_{ik} and a_{ikj}^s are the values of the output experimental variables and the values predicted by the neural network that corresponds to scenario j, respectively.

The regression procedure was maintained whenever the relative error (RE) was lower than 10^{-4}. The RE was defined as follows:

$$RE = \left| \frac{(\chi_k^2)_{j+1} - (\chi_k^2)_j}{(\chi_k^2)_j} \right| \quad (2)$$

being j the number of iterations in the non-linear regression procedure, comparing the results of the prediction made by the ANN in the scenario j and the scenario $j + 1$.

Once the fitting process for a given scenario is finished, the above-defined function χ_j^2, the Pearson's ratio coefficient for the model, r, and the root mean squared error ($RSME$) were collected. The $RMSE$ was defined as:

$$RMSE_j = \sqrt{\frac{\chi_j^2}{M}} \quad (3)$$

To minimize overfitting in the validation process, a discrimination procedure was established. For this purpose, a function presented by Equation (1) was defined for the experiments used for the validation (m_V), obtaining Equation (4):

$$\left(\chi_j^2\right)_V = \sum_{i=1}^{m_V} \left[\sum_{k=1}^{n} \left(y_{ik} - a_{ikj}^s \right)^2 \right] \quad (4)$$

This way, a new function was defined from Equations (1) and (4):

$$\left(\chi_j^2\right)_T = \chi_j^2 + \left(\chi_j^2\right)_V \quad (5)$$

Finally, a non-linear regression was performed with the selected model until a new value of RE lower than 10^{-6} was reached. With the values of the parameters finally obtained, the validation procedure was completed. In both cases, the final fitting and validation, the above defined function χ_j^2 plus those defined for each output variable k, can be expressed as χ_{jk}^2:

$$\chi_{jk}^2 = \sum_{i=1}^{m} \left(y_{ik} - a_{ikj}^s \right)^2 \quad (6)$$

To generate a consistent ANN, the data obtained through Aspen Adsorption™ was randomly divided into two groups: (i) 80% of the breakthrough curves were used for ANNs training, and (ii) 20% of them were used for validation.

The MS Excel-VBA application described above was able to compute the Pearson's ratio coefficient for the model, r, the Shapley values through the Kernel SHAP approximation [59], and the dimensionless sensitivity values derived from the partial derivatives method [60]. In this study, the latter was used for comparative purposes. Figure 2 shows a schematic representation of the computational procedure described above.

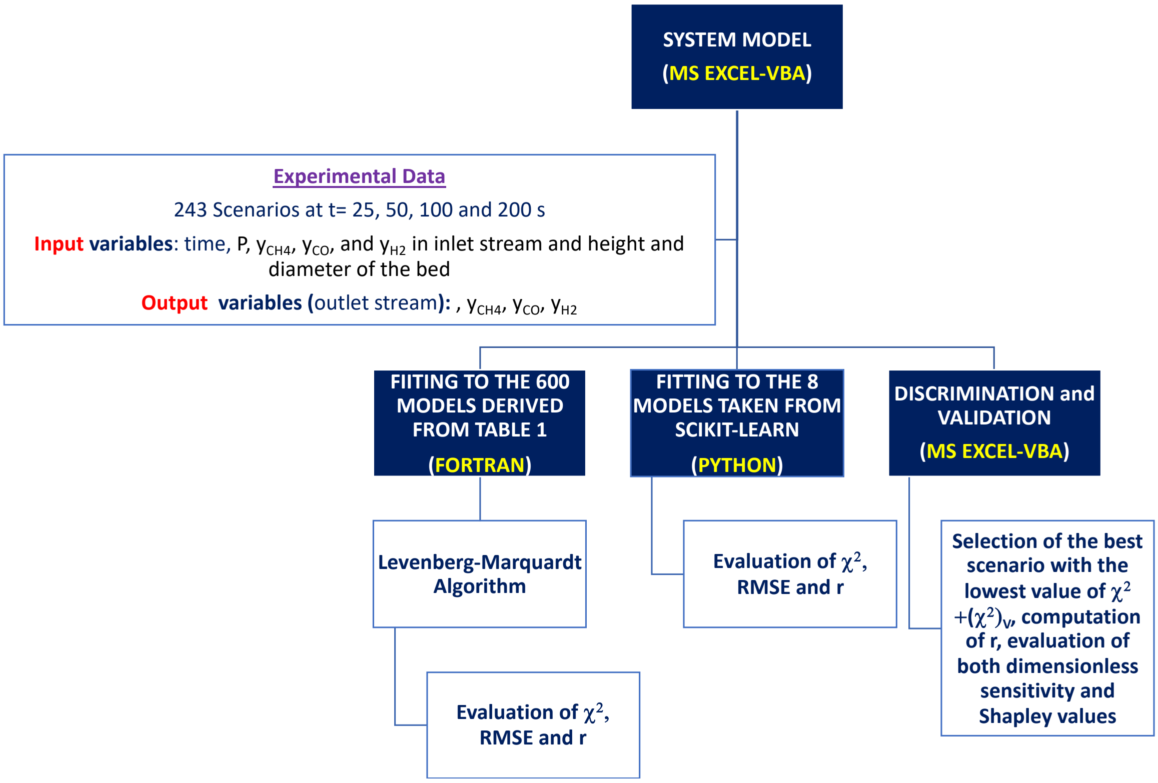

Figure 2. Block diagram of the numerical procedure followed for selecting the best model for representing breakthrough curves.

An important issue of this fitting process is the time required to fit the huge number of data. Taking as a reference the set of data corresponding to a time on stream of 200 s, about 50,000 data consisting of seven independent variables and three dependent ones were fitted to the 608 models in a time lower than 3 h using a computer with an Intel Core i7-12700K processor. This time included the discrimination and validation processes.

The results listed in Tables 2–4 and Table S1 include a nomenclature to identify a particular ANN. For example, 7-SWISH-3-HTANSIG-4-LINEAR-3 represents a ANN with three layer of neurons: the first one receives the 7 input variables and contains 3 neurons with a Swish activation function, the second one receives the 3 inputs from the first one and contains 4 neurons with a Hyperbolic Tangent Sigmoid activation function; and, the third one receives 4 inputs from the second one and contains 3 neurons (coincidental with the number of output variables of the system: molar fractions of the three species involved) with a Linear activation function. Figure 3 shows as an example the representation of the 7-SWISH-3-HTANSIG-4-LINEAR-3 artificial neural network.

Table 2. The best five ANN models that fitted a breakthrough curve obtained with Aspen Adsorption™ for the following input variables: bed height, 1 m; bed diameter, 0.015 m; pressure, 2000 kPa; molar fractions of CH_4, CO and H_2, 0.35, 0.14, 0.51, respectively.

Order	Model	RMSE	$(r^2)_{training}$	$(\chi^2)_T$
1	7-RELU-4-SWISH-4-LINEAR-3	1.474×10^{-2}	0.988	4.365×10^{-2}
2	7-RELU-4-SWISH-5-LINEAR-3	1.483×10^{-2}	0.987	4.421×10^{-2}
3	7-ELU-5-POL-5-LINEAR-3	1.987×10^{-2}	0.977	7.936×10^{-2}
4	7-RELU-4-RELU-2-LINEAR-3	2.018×10^{-2}	0.977	8.184×10^{-2}
5	7-RELU-2-ELU-4-LINEAR-3	2.025×10^{-2}	0.976	8.214×10^{-2}

Table 3. Best ANN models that fitted the data obtained with each of the time on stream. Number of breakthrough curves for training: 194. Number of breakthrough curves for validation: 49.

Model	RMSE	$(r^2)_{training}$	$(\chi^2)_T$	$(r^2)_{validation}$
Time on stream = 25 s Number of data for training = 5044. Number of data for validation = 1274				
7-RELU-3- HTANSIG-3-LINEAR-3	1.556×10^{-2}	0.986	1.487	0.903
Time on stream = 50 s Number of data for training = 9894. Number of data for validation = 2499				

Model	RMSE	$(r^2)_{training}$	$(\chi^2)_T$	$(r^2)_{validation}$
7-SWISH-3-POL-3-LINEAR-3	5.303×10^{-2}	0.916	3.646×10	0.903
Time on stream = 100 s				
Number of data for training = 19,594. Number of data for validation = 4949				
Model	RMSE	$(r^2)_{training}$	$(\chi^2)_T$	$(r^2)_{validation}$
7-ELU-5-LINEAR-3	2.311×10^{-2}	0.990	1.363×10	0.987
Time on stream = 200 s				
Number of data for training = 38,994.Number of data for validation = 9849				
Model	RMSE	$(r^2)_{training}$	$(\chi^2)_T$	$(r^2)_{validation}$
7-RELU-2-HTANSIG-4-LINEAR-3	7.339×10^{-2}	0.906	2.629×10^2	0.907

Table 4. Relative importance in percentage for each set of times on stream data of the independent variables (inputs) in each dependent variable (outputs) evaluated by the partial derivates method [60].

Time on Stream = 25 s			
	Outputs		
Inputs	$(y_{CH4})_{outlet}$	$(y_{CO})_{outlet}$	$(y_{H2})_{outtlet}$
Time (s)	43.16 (+)	43.16 (+)	43.16 (−)
Height of the bed (m)	1.87 (−)	1.87 (−)	1.87 (+)
Bed diameter (m)	0.10 (−)	0.10 (−)	0.10 (+)
Pressure (kPa)	54.39 (+)	54.39 (+)	54.39 (−)
$(y_{CH4})_{inlet}$	0.27 (+)	0.27 (+)	0.27 (−)
$(y_{CO})_{inlet}$	0.04 (+)	0.04 (+)	0.04 (−)
$(y_{H2})_{inlet}$	0.17 (+)	0.17 (+)	0.17 (−)
Time on Stream = 50 s			
	Outputs		
Inputs	$(y_{CH4})_{outlet}$	$(y_{CO})_{outlet}$	$(y_{H2})_{outtlet}$
Time (s)	62.52 (+)	53.72 (+)	60.97 (−)
Height of the bed (m)	1.56 (−)	2.30 (−)	1.69 (+)
Bed diameter (m)	0.10 (−)	0.06 (−)	0.09 (+)
Pressure (kPa)	29.26 (+)	36.29 (+)	30.51 (−)
$(y_{CH4})_{inlet}$	1.31 (−)	1.74 (−)	1.38 (+)
$(y_{CO})_{inlet}$	0.33 (−)	0.29 (−)	0.32 (+)
$(y_{H2})_{inlet}$	4.92 (−)	5.60 (−)	5.04 (+)
Time on Stream = 100 s			
	Outputs		
Inputs	$(y_{CH4})_{outlet}$	$(y_{CO})_{outlet}$	$(y_{H2})_{outtlet}$
Time (s)	73.32 (+)	80.98 (+)	74.70 (−)
Height of the bed (m)	2.18 (−)	2.51 (−)	2.24 (+)
Bed diameter (m)	0.05 (−)	0.06 (−)	0.05 (+)
Pressure (kPa)	23.72 (+)	15.96 (+)	22.33 (−)
$(y_{CH4})_{inlet}$	0.35 (+)	0.10 (+)	0.30 (−)
$(y_{CO})_{inlet}$	0.01 (+)	0.11 (+)	0.03 (−)
$(y_{H2})_{inlet}$	0.37 (−)	0.28 (−)	0.35 (+)
Time on Stream = 200 s			
	Outputs		
Inputs	$(y_{CH4})_{outlet}$	$(y_{CO})_{outlet}$	$(y_{H2})_{outtlet}$
Time (s)	77.39 (+)	76.49 (+)	77.21 (−)
Height of the bed (m)	4.30 (−)	4.68 (−)	4.38 (+)
Bed diameter (m)	0.24 (−)	0.21 (−)	0.23 (+)
Pressure (kPa)	16.85 (+)	18.09 (+)	17.10 (−)
$(y_{CH4})_{inlet}$	0.52 (+)	0.36 (+)	0.48 (−)
$(y_{CO})_{inlet}$	0.03 (+)	0.04 (+)	0.04 (−)
$(y_{H2})_{inlet}$	0.67 (−)	0.13 (−)	0.56 (+)

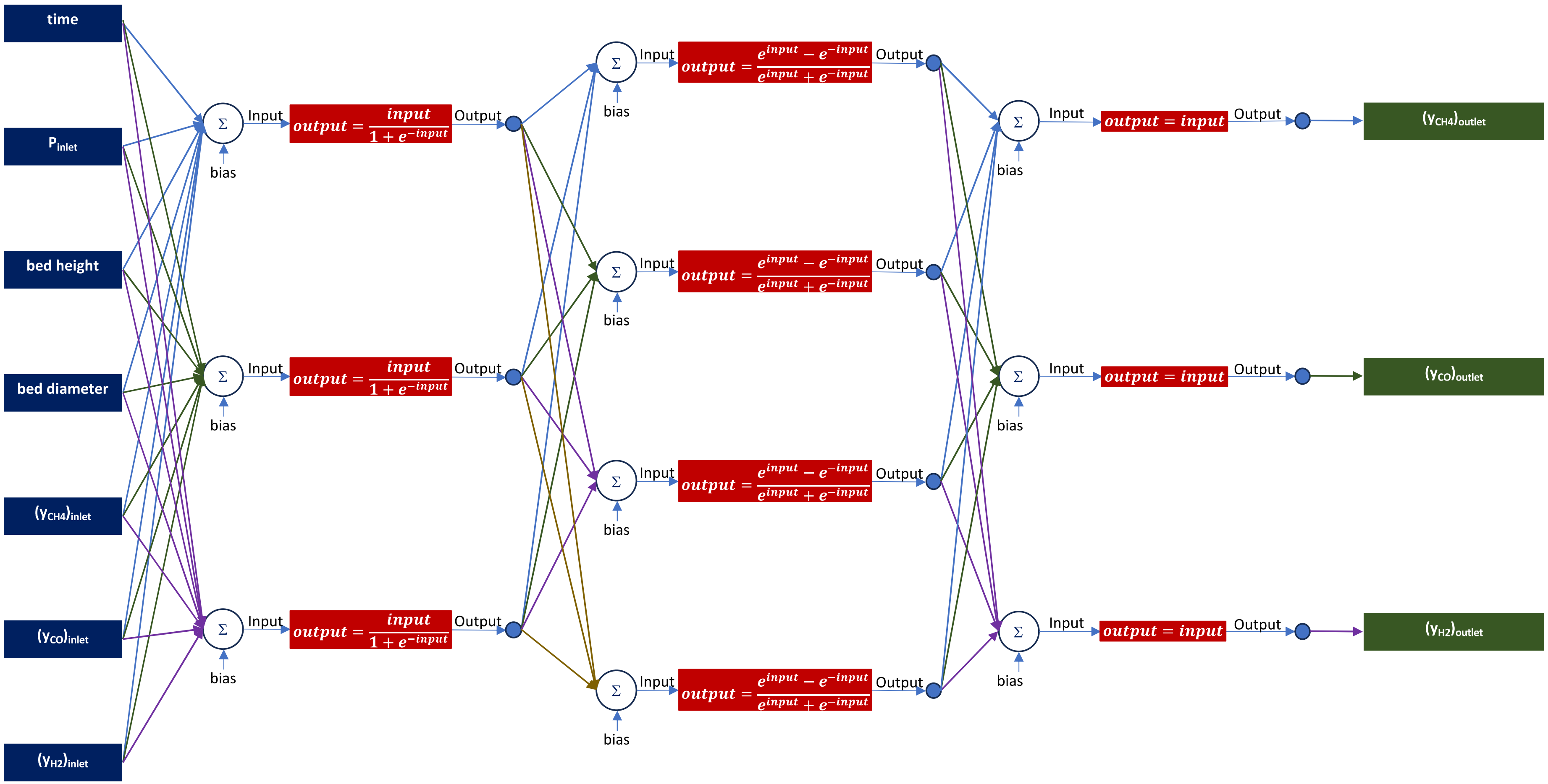

Figure 3. Representation of the 7-SWISH-3-HTANSIG-4-LINEAR-3 artificial neural network.

3. Results

As above mentioned, 243 scenarios were generated with Aspen Adsorption™ by using data taken and adapted from literature [53]. The adsorbent considered was a mixture with the same amount by weight of zeolite and activated carbon. Figure 4 shows the general physical parameters used by Aspen Adsorption™. Table 5 lists the properties of the inlet stream to the process (Feed in Figure 1) whereas Table 6 does the values of the parameters used for generating all the scenarios.

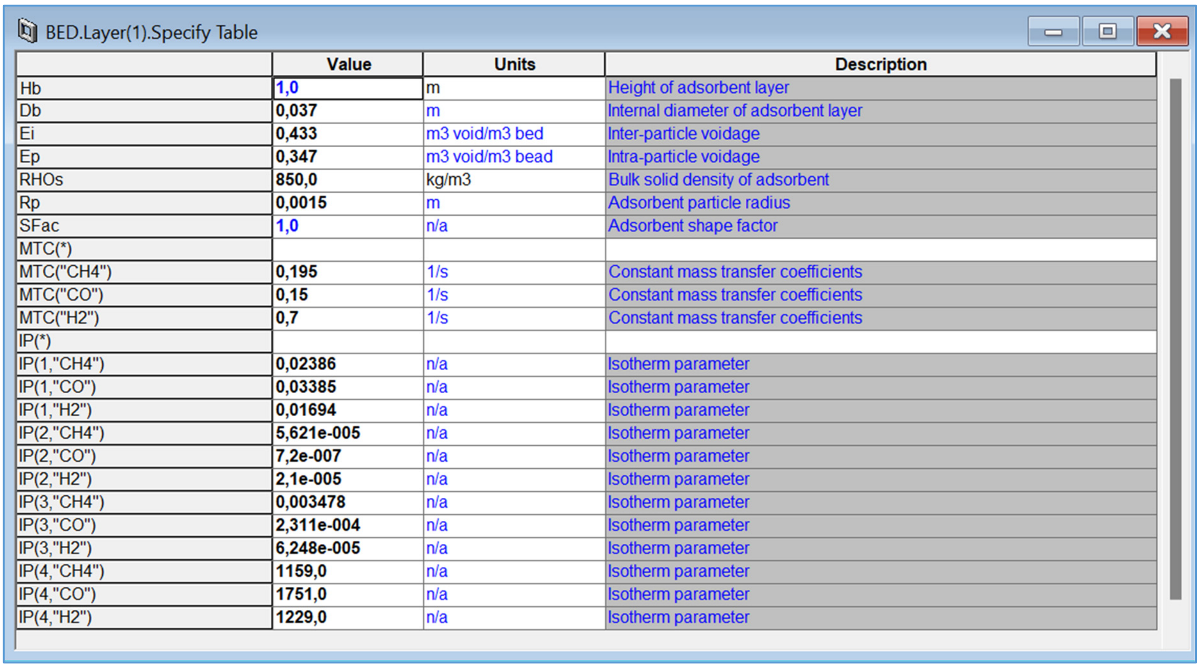

BED.Layer(1).Specify Table

	Value	Units	Description
Hb	1,0	m	Height of adsorbent layer
Db	0,037	m	Internal diameter of adsorbent layer
Ei	0,433	m3 void/m3 bed	Inter-particle voidage
Ep	0,347	m3 void/m3 bead	Intra-particle voidage
RHOs	850,0	kg/m3	Bulk solid density of adsorbent
Rp	0,0015	m	Adsorbent particle radius
SFac	1,0	n/a	Adsorbent shape factor
MTC(*)			
MTC("CH4")	0,195	1/s	Constant mass transfer coefficients
MTC("CO")	0,15	1/s	Constant mass transfer coefficients
MTC("H2")	0,7	1/s	Constant mass transfer coefficients
IP(*)			
IP(1,"CH4")	0,02386	n/a	Isotherm parameter
IP(1,"CO")	0,03385	n/a	Isotherm parameter
IP(1,"H2")	0,01694	n/a	Isotherm parameter
IP(2,"CH4")	5,621e-005	n/a	Isotherm parameter
IP(2,"CO")	7,2e-007	n/a	Isotherm parameter
IP(2,"H2")	2,1e-005	n/a	Isotherm parameter
IP(3,"CH4")	0,003478	n/a	Isotherm parameter
IP(3,"CO")	2,311e-004	n/a	Isotherm parameter
IP(3,"H2")	6,248e-005	n/a	Isotherm parameter
IP(4,"CH4")	1159,0	n/a	Isotherm parameter
IP(4,"CO")	1751,0	n/a	Isotherm parameter
IP(4,"H2")	1229,0	n/a	Isotherm parameter

Figure 4. Physical properties of the fixed bed used as the reference.

Table 5. Properties of the inlet stream to the process (Feed in Figure 1).

Variable	Value
Molar Flowrate (mol/s)	5
Temperature (K)	298.15
Pressure (kPa)	980
y_{CH4}	0.281
y_{CO}	0.115
y_{H2}	0.604

Table 6. Values of the parameters used for generating all the scenarios analyzed (243). The temperature and the molar flowrate were fixed at 298.15 K and 5 mol/s, respectively. Pressures and molar fractions are those of the inlet stream.

Variable	Values		
Pressure (kPa)	900	1480	2000
Height of the bed (m)	0.5	1	2
Bed diameter (m)	0.015	0.037	0.050
$(y_{CH4})_{inlet}$	0.25	0.30	0.35
$(y_{CO})_{inlet}$	0.08	0.11	0.14
$(y_{H2})_{inlet}$	$1 - y_{CH4} - y_{CO}$	$1 - y_{CH4} - y_{CO}$	$1 - y_{CH4} - y_{CO}$

By modifying the final time of the simulation, the number of data generated in each case was different. As mentioned above, data of the 243 scenarios were recorded each second of the simulation run, 80% of the breakthrough curves being used for ANNs training, whereas 20% of them being used for validation. Thus, for a value of this variable of 25 s, the number of data collected was 6318; for a value of 50 s, the number of data was 12,393, for a value of 100 s, the number of data was 24,543; and for a value of 200 s, the number of data was 48,843.

4. Discussion

Figure 5 shows the breakthrough curve generated by Aspen Adsorption™ for a time on stream of 600 s taken as a reference to the inlet conditions listed in Table 5. It can be seen that the steady state values for the molar fractions of CH_4, CO and H_2 in the effluent coming from the process were mostly attained at a time on stream lower than 200 s. Similar trends were observed for the rest of the runs. This time was considered the higher value for the analysis performed in this work.

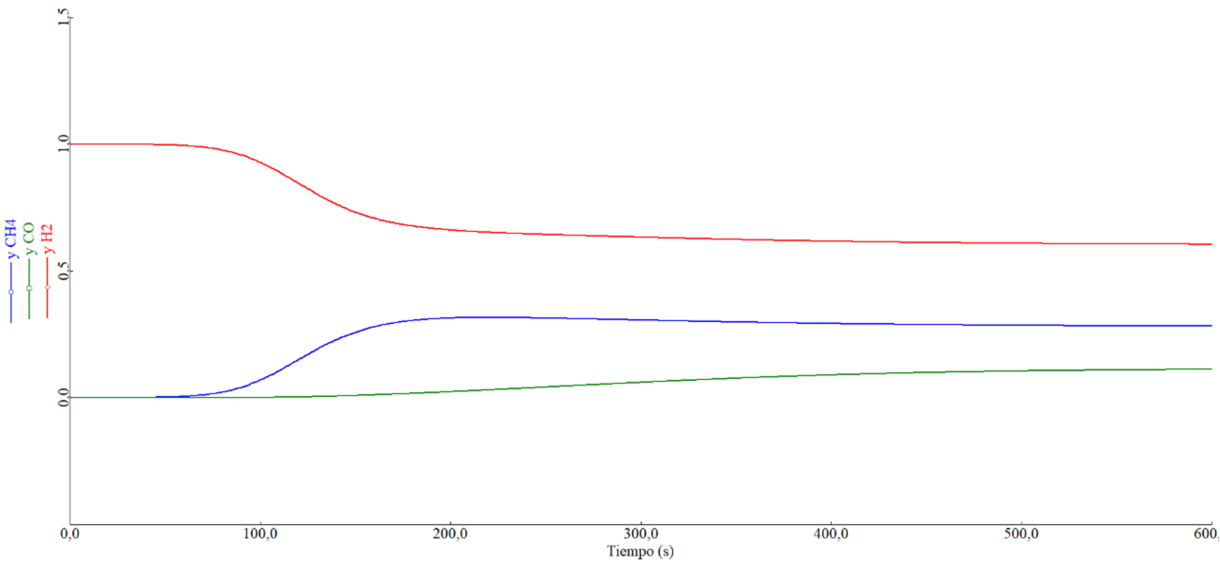

Figure 5. Evolution of the molar fractions of CH_4, CO and H_2 in the effluent for a time on stream of 600 s. The conditions of the inlet stream are listed in Table 2. Image taken from Aspen Adsortpion™.

First of all, it was checked that the procedure raised was able to work for a single breakthrough curve. As shown in Figure 6, it was found a model (7-RELU-4-SWISH-4-LINEAR-3) that fitted it well, demonstrating the capability of the procedure followed for predicting single breakthrough curves. Table 2 lists the five best ANN models that fitted the data obtained from the simulation performed by Aspen Adsorption™. Similar results were obtained when other single breakthrough curves were fitted.

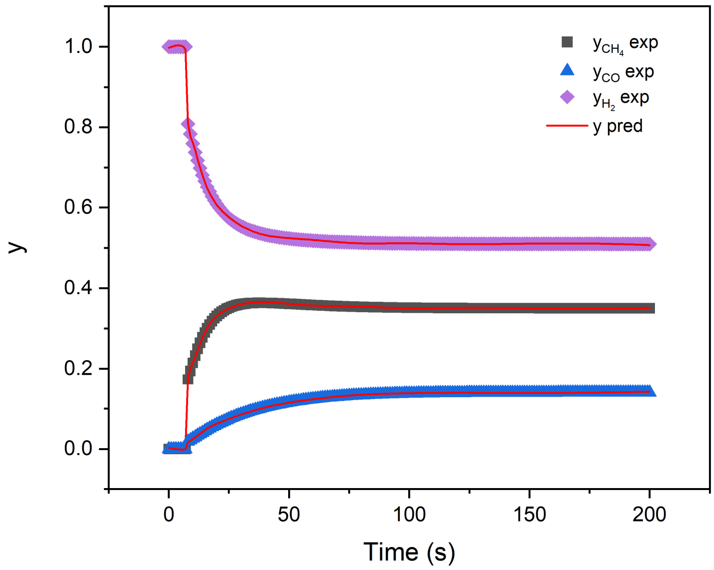

Figure 6. Breakthrough curve obtained with Aspen Adsorption™ for CH_4, CO and H_2 and predicted results for a single breakthrough curve. Input variables: bed height, 1 m; bed diameter, 0.015 m; pressure, 2000 kPa; molar fractions of CH_4, CO and H_2, 0.35, 0.14, 0.51, respectively.

Then, 80% of the breakthrough curves data for times on stream of 25, 50, 100, and 200 s were fitted to the 608 ANN models selected in this work. Table 3 shows the best ANN models that fitted the data obtained with each of the time on stream considered. Table S1 lists, as an example, the five best models for a time on stream of 100 s. It can be observed that different best ANN models were selected as a function of the time on stream considered. In general, the determination coefficient is in some cases as high as those obtained for a single breakthrough curve. However, the values of this coefficient for the validation process for all the times on stream considered were lower. Figures 7–9 show for some runs used for validation the quality of prediction reached with the best models considered for each time on stream. As checked, the capacity of the ANN for predicting breakthrough curves is not as good as expected, although the trends followed by the prediction curves could be used to make a good estimation of the dynamic behaviour of the adsorption process.

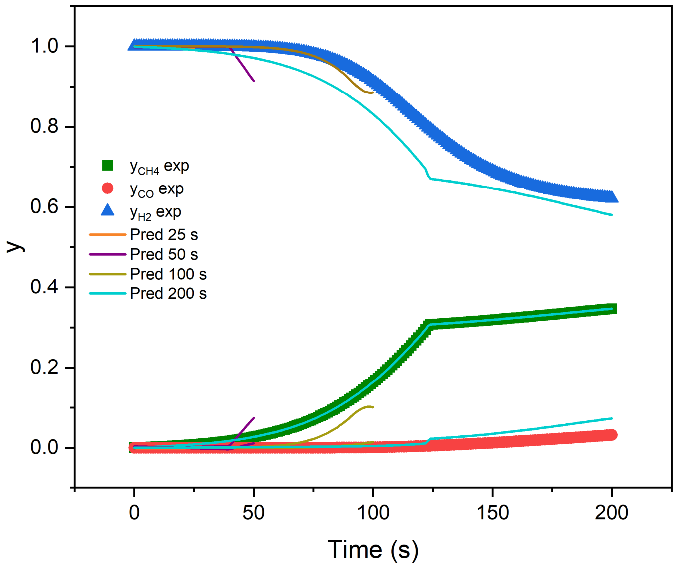

Figure 7. Breakthrough curves obtained with Aspen Adsorption™ for CH_4, CO and H_2 and predicted results at times on stream of 25, 50, 100 and 200 s. Input variables: bed height, 1 m; bed diameter, 0.037 m; pressure, 900 kPa; molar fractions of CH_4, CO and H_2, 0.30, 0.14, 0.56, respectively. This run was in the pack of runs used for validation.

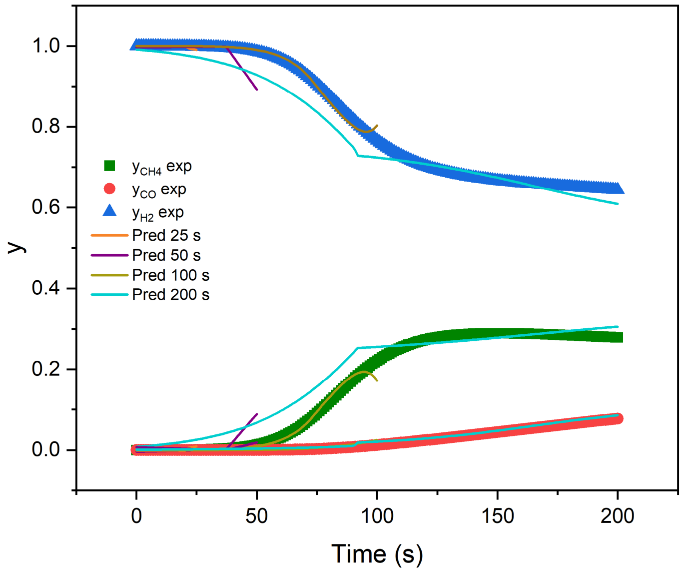

Figure 8. Breakthrough curves obtained with Aspen Adsorption™ for CH_4, CO and H_2 and predicted results at times on stream of 25, 50, 100 and 200 s. Input variables: bed height, 1 m; bed diameter, 0.037 m; pressure, 2000 kPa; molar fractions of CH_4, CO and H_2, 0.25, 0.14, 0.61, respectively. This run was in the pack of runs used for validation.

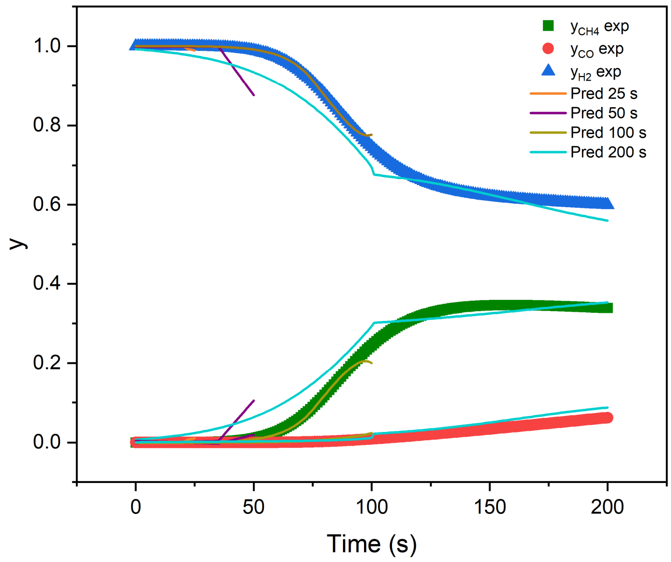

Figure 9. Breakthrough curves obtained with Aspen Adsorption™ for CH_4, CO and H_2 and predicted results at times on stream of 25, 50, 100 and 200 s. Input variables: bed height, 1 m; bed diameter, 0.037 m; pressure, 1480 kPa; molar fractions of CH_4, CO and H_2, 0.30, 0.14, 0.56, respectively. This run was in the pack of runs used for validation.

On the other hand, Table 4 shows the relative importance of the independent variables (inputs) in each dependent variable (outputs) evaluated by the partial derivates method [60]. If the positive variation of an independent variable led to a positive variation of a dependent one the sign would be +; in the contrary case, it would be −. It can be observed that the relative importance of each dependent variable for all the sets of experiments considered was mainly a function of the time on stream and the pressure. It was also observed that the sign of some matches of independent and dependent variables was also a function of the set of time on stream considered.

In summary, the results obtained in this study showed that although the ANN models can be used to predict the behaviour of breakthrough curves of multicomponent adsorption processes, the quality of the prediction was not as good as expected when the number of breakthrough curves considered was different from one.

Finally, an ANN model was used to predict the breakthrough times corresponding to the reduction of the H_2 concentration in the outlet stream of 2% for all the scenarios raised. Again, 80% of the values obtained by simulation were used for training, whereas the remaining ones were used for validation. Table 7 shows the best ANN model, whereas Table 8 lists the relative importance of the independent variables (inputs) on the dependent variable (breakthrough time) evaluated by the partial derivates method. Again, the main input variable affecting the breakthrough time was the pressure, the sign being negative. Figure 10 shows a comparison between the values of the breakthrough times computed by Aspen Adsorption™ and used for validation and those predicted by the best ANN model. As confirmed by the $(r^2)_{validation}$ value, a good agreement between both sets of values was reached.

Table 7. Best ANN model that fitted the breakthrough times.

Model	RMSE	$(r^2)_{training}$	$(\chi^2)_T$	$(r^2)_{validation}$
7-POL-4-ELU-3-LINEAR-1	8.319×10^{-1}	0.9998	1.457×10^{2}	0.9998

Table 8. Relative importance in percentage for each set of times on stream data of the independent variables (inputs) on the dependent variable (breakthrough time) evaluated by the partial derivates method [60].

Inputs	Output
	Breakthrough Time
Height of the Bed (m)	0.37 (+)
Bed Diameter (m)	0.00 (0)
P (kPa)	99.58 (−)
y_{CH4}	0.00 (0)
y_{CO}	0.00 (0)
y_{H2}	0.00 (0)

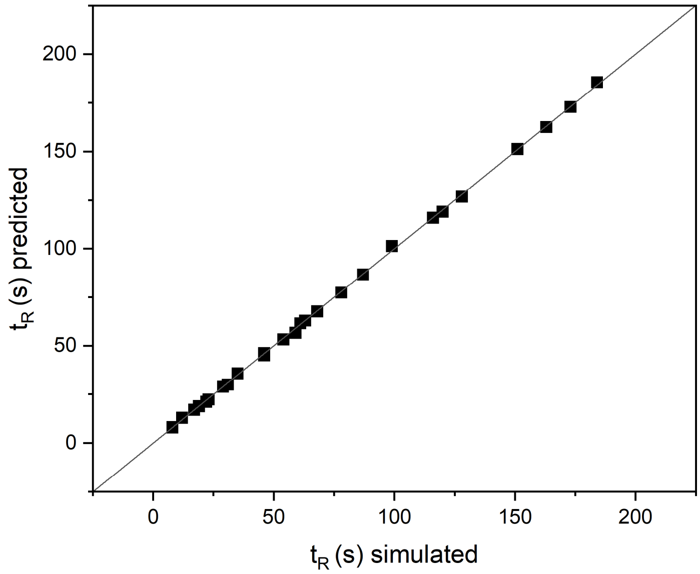

Figure 10. Comparison between the values of the breakthrough times computed by Aspen Adsorption^{TM} and used for validation and those predicted by the best ANN model.

The methodology here presented for the analysis of adsorption processes can be easily extrapolated to other separation or conversion processes and for the computation of thermodynamic properties. Two studies are currently running which take advantage of the experience here acquired: prediction of thermodynamical properties from COnductor-like Screening Model (COSMO) computations and evaluation of the sensitivity of characterization properties of catalysts on their catalytic performance.

5. Conclusions

This work analyzes the reliability of ANNs to predict a complex process. This way, breakthrough curves and breakthrough times of the multicomponent adsorption of H_2, CO and CO_2 in a fixed bed from a large set of runs (rather than a single run, which is the majority situation reported in the literature) generated through Aspen AdsorptionTM. As an example, a system constituted by a stream containing H_2, CO and CO_2 was considered. Thus, 243 different scenarios were generated with the software mentioned above. From them, it was selected sets of data depending on the ending time of the simulation: 25, 50, 100 and 200 s. The different sets were fitted to 600 ANNs configurations through a homemade software running in Fortran. Eight additional algorithms contained in the Scikit-Learn, a Python module for machine learning, were also considered. To generate a consistent ANN, the data obtained through Aspen Adsorption^{TM} was randomly divided into two groups: (i) 80% of the breakthrough curves and breakthrough times, which were used for ANNs training, and (ii) 20% of them, which were used for validation. After checking that the procedure raised was able to work for a single breakthrough curve, it was observed that the capacity of the ANN for predicting a set of breakthrough curves was not so good as expected although the trends followed by the prediction curves could be used to make a good estimation of the dynamic behaviour of adsorption process. Finally, ANN models were used to predict the breakthrough times corresponding to the reduction of the H_2 concentration in the outlet stream of 2% for all the scenarios raised. A good agreement was observed between the values of the breakthrough times computed by Aspen Adsorption^{TM} and used for validation and those predicted by the best ANN model. The general procedure followed here could be equally used for analyzing a real set of adsorption experiments or other different complex processes as described here.

Supplementary Materials

The additional data and information can be downloaded at: https://www.sciltp.com/journals/acpa/2025/1/725/s1. References [61–64] are cited in the supplementary materials.

Author Contributions

Conceptualization, J.L.V. and A.G.-F.; methodology, V.R.F. and M.M.R.-D.; software, J.L.V.; data curation, V.R.F. and A.G.-F.; writing—original draft preparation, J.L.V. and V.R.F.; visualization, V.R.F. and M.M.R.-D.; investigation, all; supervision, V.R.F. and J.L.V.; software, validation, J.L.V. and M.M.R.-D.; writing—review and editing, V.R.F. and A.G.-F. All authors have read and agreed to the published version of the manuscript.

Funding

This research received no external funding.

Data Availability Statement

The original contributions presented in the study are included in the article and Supplementary Materials; further inquiries can be directed to the corresponding author.

Conflicts of Interest

The authors declare no conflict of interest.

References

1. Cavalcanti, F.M.; Kozonoe, C.E.; Pacheco, K.A.; et al. Application of Artificial Neural Networks to Chemical and Process Engineering. *Deep. Learn. Appl.* **2021**, *2021*, 167.
2. Feise, H.J.; Schaer, E. Mastering Digitized Chemical Engineering. *Educ. Chem. Eng.* **2021**, *34*, 78–86. https://doi.org/10.1016/j.ece.2020.11.011.
3. Venkatasubramanian, V. The Promise of Artificial Intelligence in Chemical Engineering: Is It Here, Finally? *AIChE J.* **2019**, *65*, 466.
4. Barbero-Sánchez, J.; Megía-Ortega, A.; Ferro, V.R.; et al. Exploring Alternatives to Create Digital Twins from and for Process Simulation. *J. Comput. Sci. Res.* **2024**, *6*, 16–30.
5. García, N.M.; Valverde, J.L.; Cano, B.D.; et al. Selective Recovery of Zinc from Alkaline Batteries via a Basic Leaching Process and the Use of a Machine Learning-Based Digital Twin for Predictive Purposes. *Energies* **2024**, *17*, 1–15.
6. Li, C.; Yang, T.; Luo, H.; et al. Multi-Objective Optimization of Breakthrough Times for Hydrogen Purification through Layered Bed Pressure Swing Adsorption Based on Genetic Algorithm and Artificial Neural Network Model. *Int. J. Hydrogen Energy* **2024**, *52*, 390–405. https://doi.org/10.1016/j.ijhydene.2023.08.357.
7. Babu, B.V.; Ramakrishna, V.; Chakravarthy, K.K. Artificial Neural Networks for Modeling of Adsorption. *Learning* **2008**, *5*, 1–6.
8. Arora, A.; Iyer, S.S.; Hasan, M.M.F. Computational Material Screening Using Artificial Neural Networks for Adsorption Gas Separation. *J. Phys. Chem. C* **2020**, *124*, 21446–21460. https://doi.org/10.1021/acs.jpcc.0c05900.
9. Ma, S.; Tong, L.; Ye, F.; et al. Hydrogen Purification Layered Bed Optimization Based on Artificial Neural Network Prediction of Breakthrough Curves. *Int. J. Hydrogen Energy* **2019**, *44*, 5324–5333. https://doi.org/10.1016/j.ijhydene.2018.12.142.
10. Díaz-Rivera, A.; Zavala-Arce, R.E.; García-Rivas, J.L.; et al. Modeling of Artificial Neural Networks for the Adsorption of Synthetic Dyes in an Aqueous Solution Using Double Layer Hydroxides. *MRS Adv.* **2023**, *8*, 77–82. https://doi.org/10.1557/s43580-023-00535-z.
11. Astray, G.; Soria-Lopez, A.; Barreiro, E.; et al. Machine Learning to Predict the Adsorption Capacity of Microplastics. *Nanomaterials* **2023**, *13*, 1061. https://doi.org/10.3390/nano13061061.
12. Schio, R.R.; Salau, N.P.G.; Mallmann, E.S.; et al. Modeling of Fixed-Bed Dye Adsorption Using Response Surface Methodology and Artificial Neural Network. *Chem. Eng. Commun.* **2021**, *208*, 1081–1092.
13. Chowdhury, S.; Das Saha, P. Artificial Neural Network (ANN) Modeling of Adsorption of Methylene Blue by NaOH-Modified Rice Husk in a Fixed-Bed Column System. *Environ. Sci. Pollut. Res.* **2013**, *20*, 1050–1058. https://doi.org/10.1007/s11356-012-0912-2.
14. Yusuf, M.; Song, K.; Li, L. Fixed Bed Column and Artificial Neural Network Model to Predict Heavy Metals Adsorption Dynamic on Surfactant Decorated Graphene. *Colloids Surf. A Physicochem. Eng. Asp.* **2020**, *585*, 124076. https://doi.org/10.1016/j.colsurfa.2019.124076.
15. Senthilkumar, V.; Ilavenil, K.K. Artificial Neural Network Prediction of Optimal Phenylic Acid Adsorption Using Lantana Camara Activated Carbon. *Orient. J. Chem.* **2023**, *39*, 172–178. https://doi.org/10.13005/ojc/390121.
16. Hou, J.; Bao, W.; Zhang, J.; et al. Characteristics and Mechanisms of Sulfamethoxazole Adsorption onto Modified Biochars with Hierarchical Pore Structures: Batch, Predictions Using Artificial Neural Network and Fixed Bed Column Studies. *J. Water Process Eng.* **2023**, *54*, 103975. https://doi.org/10.1016/j.jwpe.2023.103975.
17. Meena, G.; Rawal, N. Artificial Neural Network Modeling for Adsorption Efficiency of Cr(VI) Ion from Aqueous Solution Using Waste Tire Activated Carbon. *Nat. Environ. Pollut. Technol.* **2023**, *22*, 1481–1491. https://doi.org/10.46488/NEPT.2023.v22i03.033.
18. Atta, H.A.M. Artificial Neural Network [ANN] Modeling for Tetracycline Adsorption on Rice Husk Using Continuous System. *Desalination Water Treat.* **2024**, *317*, 100026. https://doi.org/10.1016/j.dwt.2024.100026.

19. Nighojkar, A.; Zimmermann, K.; Ateia, M.; et al. Application of Neural Network in Metal Adsorption Using Biomaterials (BMs): A Review. *Environ. Sci. Adv.* **2022**, *2*, 11–38. https://doi.org/10.1039/d2va00200k.
20. Zafari, T.; Keyvani, B.; Mousavi, M.; et al. Adsorption of Cyclohexane onto Activated Nanoporous Graphene: Modeling Using Artificial Neural Network. *Iran. J. Chem. Chem. Eng.* **2023**, *42*, 772–785.
21. Reynel-Ávila, H.E.; Aguayo-Villarreal, I.A.; Diaz-Muñoz, L.L.; et al. A Review of the Modeling of Adsorption of Organic and Inorganic Pollutants from Water Using Artificial Neural Networks. *Adsorpt. Sci. Technol.* **2022**, *2022*, 9384871. https://doi.org/10.1155/2022/9384871.
22. Ghaedi, A.M.; Vafaei, A. Applications of Artificial Neural Networks for Adsorption Removal of Dyes from Aqueous Solution: A Review. *Adv. Colloid Interface Sci.* **2017**, *245*, 20–39. https://doi.org/10.1016/j.cis.2017.04.015.
23. Subraveti, S.G.; Li, Z.; Prasad, V.; et al. Physics-Based Neural Networks for Simulation and Synthesis of Cyclic Adsorption Processes. *Ind. Eng. Chem. Res.* **2022**, *61*, 4095–4113. https://doi.org/10.1021/acs.iecr.1c04731.
24. Tariq, R.; Abatal, M.; Vargas, J.; et al. Deep Learning Artificial Neural Network Framework to Optimize the Adsorption Capacity of 3-Nitrophenol Using Carbonaceous Material Obtained from Biomass Waste. *Sci. Rep.* **2024**, *14*, 20250. https://doi.org/10.1038/s41598-024-70989-0.
25. Göde, F.; Yılmaz, A.; Aktaş, A.H.; et al. Artificial Neural Network Approach to Model Cr(III) and Cr(VI) Adsorption by NCS, ACS and BCS. *Appl. Water Sci.* **2024**, *14*, 28. https://doi.org/10.1007/s13201-023-02054-6.
26. Mesutoğlu, Ö.Ç. The Use of Artificial Neural Network for Modeling Adsorption of Congo Red Onto Activated Hazelnut Shell. *Environ. Monit. Assess.* **2024**, *196*, 630. https://doi.org/10.21203/rs.3.rs-3804393/v1.
27. Iftikhar, S.; Zahra, N.; Rubab, F.; et al. Artificial Neural Networks for Insights into Adsorption Capacity of Industrial Dyes Using Carbon-Based Materials. *Sep. Purif. Technol.* **2023**, *326*, 124891. https://doi.org/10.1016/j.seppur.2023.124891.
28. Cong, G.; Gupta, A.; Neumann, R.; et al. Prediction of CO_2 Adsorption in Nano-Pores with Graph Neural Networks. In Proceedings of the AAAI Conference on Artificial Intelligence, Online, 22 February–1 March 2022.
29. Chen, S.; Bai, S.; Ya, R.; et al. Continuous Silicic Acid Removal in a Fixed-Bed Column Using a Modified Resin: Experiment Investigation and Artificial Neural Network Modeling. *J. Water Process Eng.* **2022**, *49*, 102937. https://doi.org/10.1016/j.jwpe.2022.102937.
30. Giri, A.K.; Mishra, P.C. Application of Artificial Neural Network for Prediction of Fluoride Removal Efficiency Using Neutralized Activated Red Mud from Aqueous Medium in a Continuous Fixed Bed Column. *Environ. Sci. Pollut. Res.* **2023**, *30*, 23997–24012. https://doi.org/10.21203/rs.3.rs-1702568/v1.
31. Lee, W.S.; Park, M.Y.; Duong, X.Q.; et al. Time Allocation of a Three-Bed Adsorption Chiller Using an Artificial Neural Network. *Case Stud. Therm. Eng.* **2021**, *28*, 101553. https://doi.org/10.1016/j.csite.2021.101553.
32. El Bey, A.; Laidi, M.; Yettou, A.; et al. Practical Artificial Neural Network Tool for Predicting the Competitive Adsorption of Dyes on Gemini Polymeric Nanoarchitecture. *Kem. Ind.* **2021**, *70*, 481–488. https://doi.org/10.15255/kui.2020.069.
33. Dalhat, M.A.; Mu'Azu, N.D.; Essa, M.H. Generalized Decay and Artificial Neural Network Models for Fixed-Bed Phenolic Compounds Adsorption onto Activated Date Palm Biochar. *J. Environ. Chem. Eng.* **2021**, *9*, 104711. https://doi.org/10.1016/j.jece.2020.104711.
34. Chen, C.; Chen, Z.; Shen, J.; et al. Dynamic Adsorption Models and Artificial Neural Network Prediction of Mercury Adsorption by a Dendrimer-Grafted Polyacrylonitrile Fiber in Fixed-Bed Column. *J. Clean. Prod.* **2021**, *310*, 127511. https://doi.org/10.1016/j.jclepro.2021.127511.
35. Hentabli, M.; Hanini, S.; Laidi, M.; et al. Artificial Neural Network Modelling of Multi-System Dynamic Adsorption of Organic Pollutants on Activated Carbon. *Kem. Ind.* **2021**, *70*, 1–12. https://doi.org/10.15255/kui.2020.011.
36. Ahmad, Z.U.; Yao, L.; Lian, Q.; et al. The Use of Artificial Neural Network (ANN) for Modeling Adsorption of Sunset Yellow onto Neodymium Modified Ordered Mesoporous Carbon. *Chemosphere* **2020**, *256*, 127081. https://doi.org/10.1016/j.chemosphere.2020.127081.
37. Khan, T.; Manan, T.S.B.A.; Isa, M.H.; et al. Modeling of Cu(II) Adsorption from an Aqueous Solution Using an Artificial Neural Network (ANN). *Molecules* **2020**, *25*, 3263. https://doi.org/10.3390/molecules25143263.
38. De Leon, V.B.; de Negreiros, B.A.F.; Brusamarello, C.Z.; et al. Artificial Neural Network for Prediction of Color Adsorption from an Industrial Textile Effluent Using Modified Sugarcane Bagasse: Characterization, Kinetics and Isotherm Studies. *Environ. Nanotechnol. Monit. Manag.* **2020**, *14*, 100387. https://doi.org/10.1016/j.enmm.2020.100387.
39. Mazloom, M.S.; Rezaei, F.; Hemmati-Sarapardeh, A.; et al. Artificial Intelligence Based Methods for Asphaltenes Adsorption by Nanocomposites: Application of Group Method of Data Handling, Least Squares Support Vector Machine, and Artificial Neural Networks. *Nanomaterials* **2020**, *10*, 890. https://doi.org/10.3390/nano10050890.
40. Anbazhagan, S.; Thiruvengadam, V.; Kulanthai, K. Adaptive Neuro-Fuzzy Inference System and Artificial Neural Network Modeling for the Adsorption of Methylene Blue by Novel Adsorbent in a Fixed-Bed Column Method. *Iran. J. Chem. Chem. Eng.* **2020**, *39*, 75–93.

41. Kiraz, A.; Canpolat, O.; Erkan, E.F.; et al. Artificial Neural Networks Modeling for the Prediction of Pb(II) Adsorption. *Int. J. Environ. Sci. Technol.* **2019**, *16*, 5079–5086. https://doi.org/10.1007/s13762-018-1798-4.
42. Yetilmezsoy, K.; Demirel, S. Artificial Neural Network (ANN) Approach for Modeling of Pb(II) Adsorption from Aqueous Solution by Antep Pistachio (*Pistacia Vera* L.) Shells. *J. Hazard. Mater.* **2008**, *153*, 1288–1300. https://doi.org/10.1016/j.jhazmat.2007.09.092.
43. Zarei, M.; Fazli, S.; Najjari, N.; et al. Efficiency of Artificial Neural Networks for Modeling of Malachite Green Adsorption by Tea Waste and Adsorption Isotherm Study. *J. Water Wastewater* **2019**, *30*, 51–62. https://doi.org/10.22093/wwj.
44. Dinçtürk Atalay, E.; Göde, F.; Aktaş, A.H. Artificial Neural Networks Approach for Modeling of Cr(VI) Adsorption from Aqueous Solution by MR, MAC, MS. *J. Interfaces* **2051**, *2*, 81–91. https://doi.org/10.22051/JITF.2018.18582.1014.
45. Yildiz, S. Artificial Neural Network Approach for Modeling of Ni(II) Adsorption from Aqueous Solution by Peanut Shell. *Ecol. Chem. Eng.* **2018**, *25*, 581–604. https://doi.org/10.1515/eces-2018-0039.
46. Bulut, A.; Yusan, S.; Aytas, S.; et al. Artificial Neural Network (ANN) Approach for Modeling of Sr(II) Adsorption from Aqueous Solution by Natural Calcium-Based Materials. *Res. J. Environ. Sci.* **2018**, *12*, 121–131. https://doi.org/10.3923/rjes.2018.121.131.
47. de Araújo Padilha, C.E.; de Araújo Padilha, C.A.; de Santana Souza, D.F.; et al. Recurrent Neural Network Modeling Applied to Expanded Bed Adsorption Chromatography of Chitosanases Produced by Paenibacillus Ehimensis. *Chem. Eng. Res. Des.* **2017**, *117*, 24–33. https://doi.org/10.1016/j.cherd.2016.09.022.
48. Sabri, N.H.; Rani, N.H.A.; Mohamad, N.F.; et al. Simulation of CO2 Capture for Amine Impregnated Activated Carbon–Palm Kernel Shell (AC-PKS) Adsorbent in Pressure Swing Adsorption (PSA) Using Aspen Adsorption. *Mater. Today Proc.* **2023**. https://doi.org/10.1016/j.matpr.2022.12.206.
49. Gabriela, A. The Potential of Aspen Adsorption TM Software Package to Simulate Pressure Swing Adsorption Units. Master's Thesis, Universidade do Porto, Porto, Portugal, 2020.
50. Kottititum, B.; Srinophakun, T.; Phongsai, N.; et al. Optimization of a Six-Step Pressure Swing Adsorption Process for Biogas Separation on a Commercial Scale. *Appl. Sci.* **2020**, *10*, 4692. https://doi.org/10.3390/app10144692.
51. Tong, L.; Bénard, P.; Zong, Y.; et al. Artificial Neural Network Based Optimization of a Six-Step Two-Bed Pressure Swing Adsorption System for Hydrogen Purification. *Energy AI* **2021**, *5*, 100075. https://doi.org/10.1016/j.egyai.2021.100075.
52. Lee, J.J.; Kim, M.K.; Lee, D.G.; et al. Heat-Exchange Pressure Swing Adsorption Process for Hydrogen Separation. *AIChE J.* **2008**, *54*, 2054–2064. https://doi.org/10.1002/aic.11544.
53. Jagtap, A.D.; Karniadakis, G.E. How Important Are Activation Functions in Regression and Classification? A Survey, Performance Comparison, and Future Directions. *J. Mach. Learn. Model. Comput.* **2023**, *4*, 21–75.
54. Alzubaidi, L.; Zhang, J.; Humaidi, A.J.; et al. Review of Deep Learning: Concepts, CNN Architectures, Challenges, Applications, Future Directions. *J. Big Data* **2021**, *8*, 1–74.
55. Reyad, M.; Sarhan, A.M.; Arafa, M. A Modified Adam Algorithm for Deep Neural Network Optimization. *Neural Comput. Appl.* **2023**, *35*, 17095–17112.
56. Hagan, M.T.; Demuth, H.B.; Beale, M. *Neural Network Design*; PWS Publishing Co.: Stillwater, OK, USA, 1997.
57. Nanni, L.; Brahnam, S.; Paci, M.; et al. Comparison of Different Convolutional Neural Network Activation Functions and Methods for Building Ensembles for Small to Midsize Medical Data Sets. *Sensors* **2022**, *22*, 6129.
58. Moré, J.J. The Levenberg-Marquardt Algorithm: Implementation and Theory. In Proceedings of the Numerical Analysis: Biennial Conference, Dundee, Scotland, 28 June–1 July 1977; Springer: Berlin/Heidelberg, Germany, 2006; pp. 105–116.
59. Aas, K.; Jullum, M.; Løland, A. Explaining Individual Predictions When Features Are Dependent: More Accurate Approximations to Shapley Values. *Artif. Intell.* **2021**, *298*, 103502.
60. De Oña, J.; Garrido, C. Extracting the Contribution of Independent Variables in Neural Network Models: A New Approach to Handle Instability. *Neural Comput. Appl.* **2014**, *25*, 859–869.
61. Hagan, M.T.; Menhaj, M.B. Training feedforward networks with the Marquardt algorithm. *IEEE Trans. Neural Netw.* **1994**, *5*, 989–993. https://doi.org/10.1109/72.329697.
62. Valverde, J.L.; Ferro, V.R.; Giroir-Fendler, A. Prediction of the solid-liquid equilibrium of ternary and quaternary salt-water systems. Influence of the e-NRTL interaction parameters. *Fluid Phase Equilib.* **2023**, *572*, 113832. https://doi.org/10.1016/j.fluid.2023.113832.
63. Valverde, J.L.; Ferro, V.R.; Giroir-Fendler, A. Application of the e-NRTL model to electrolytes in mixed solvents methanol-, ethanol-water, and PEG-water. *Fluid Phase Equilib.* **2022**, *560*, 113516. https://doi.org/10.1016/j.fluid.2022.113516.

64. Valverde, J.L.; Ferro, V.R.; Giroir-Fendler, A. Estimation of e-NRTL binary interaction parameters and its impact on the prediction of thermodynamic properties of multicomponent electrolyte systems. *Fluid Phase Equilib.* **2022**, *551*, 113264. https://doi.org/10.1016/j.fluid.2021.113264.